Bakker A., Van den Akker H.E.A. (1991) A Computational Study on Dispersing Gas in a Stirred Reactor. Proceedings of the 7th European Conference on Mixing, September 18-20, 1991, Brugge, Belgium, page 199-208. Paper also published in: "Fluid Mechanics of Mixing: Modeling, Operations and Experimental Techniques", R. King (ed.), Kluwer Academic Publishers, Dordrecht, 1992, ISBN 0-7923-1720-3, page 37-45.

A COMPUTATIONAL STUDY ON DISPERSING GAS IN A STIRRED REACTOR

A. BAKKER, H.E.A. VAN DEN AKKER, Kramers Laboratorium voor Fysische Technologie. Delft University of Technology. NL

INTRODUCTION

The numerical computation of the flow field in stirred tank reactors has received attention since the beginning of the 1980's, starting with Harvey (1980) and Harvey and Greaves (1982). Most times computations are limited to single-phase flow. Reviews of the work done on these single-phase computations have been given by Ranade and Joshi (1990) and Ranade et al. (1989). Stirred vessels are generally used for multiphase mixing but full computation of the flow field of a liquid phase in which a gas is dispersed is not yet possible. This is partly due to a lack of knowledge of bubble dynamics and the influence of bubbles on the turbulence structure, and partly due to computational limitations.

In spite of these difficulties, several attempts have been made to model the flow in a gassed stirred tank in a less rigorous way. Issa and Gosman (1981) calculated the flow in a gassed stirred vessel equipped with a Rushton turbine. In their calculations they assumed a very small (0.5 mm), constant bubble diameter. Further they used very coarse grids and it was not possible to verify the results of their simulations because of a lack of experimental data. Looney at al. (1985) presented a model for the turbulent flow of solid/liquid suspensions in stirred vessels. This model incorporated mass balance and momentum equations for both phases, together with a two-phase turbulence model. Pericleous and Patel (1987) calculated both the single-phase flow and the two-phase flow in a stirred tank. Their calculations were done for various impeller types and combinations of impellers. Due to the use of a simple one-equation k-l type turbulence model, their velocity predictions had a limited accuracy only. Their two-phase calculations were done assuming a constant bubble size and a constant bubble rise velocity, and the results could not be verified with experimental data. Mann (1988) followed a different approach. He modeled the flow created by a disc-turbine by a network of zones, and calculated the gas transport in this network by solving the continuity equation for the gas phase. Although his results were interesting and had a qualitative appeal, the simplified flow pattern makes extension of the model to other geometries difficult. An extensive model has been proposed by Trägårdh (1988). Not only did he manage to incorporate the momentum exchange between the gas phase and the liquid phase, but he also incorporated a model for local mass transfer and for the growth of microorganisms. However, his code was not capable of calculating the local bubble size and, like the other authors mentioned above, he used a constant value of the slip velocity between the gas bubbles and the liquid phase, without taking the influence of turbulence on bubble rise velocity into account.

It will be clear that there is a strong need for more extensive models, capable of calculating local gas holdup, local bubble size and local mass transfer rate. In the current research project, the general purpose code FLUENT is used for calculating the single-phase flow in a stirred vessel equipped with either an axial flow impeller or a disc-turbine. Provided that at low void fractions this overall flow pattern is not affected by the gas, this flow pattern is used as input for an in-house code named *GHOST!* (Gas Holdup Simulation Tool!) that calculates the distribution of the gas in the vessel on the basis of conservation equations. A mathematical model for bubble break-up and bubble coalescence, based on local turbulence intensity and local energy dissipation rate as calculated by FLUENT, is incorporated in this code. *GHOST!* is capable of calculating local values of void fraction, bubble size, interfacial area and mass transfer. Further details regarding the several modeling steps are given below.

SINGLE-PHASE FLOW PATTERN COMPUTATION

The single-phase flow pattern is calculated by solving the momentum equations and mass conservation equation with the aid of the general purpose code FLUENT. An Algebraic Stress Model, as described by Boysan (1984), is used for calculating the turbulent Reynolds stresses. To investigate possible grid dependence of the flow fields computations were done with several grid sizes. Two-dimensional calculations, assuming rotational symmetry, were done with 50x25, 42x27 and 28x14 grid nodes. Three-dimensional computations were done with

50x25x20, 52x27x17 and 56x35x11 grid nodes (in (z, r, ϕ) coordinates). The 3D calculations were done for a 90 degree segment of the vessel. In these computations the impellers have been treated as black boxes. For the disc turbine the u, v and w-velocities, together with the turbulent kinetic energy k and dissipation rate ε have been prescribed on the vertical swept boundary of the impeller, using symmetric, parabolic profiles according to the data presented by Ranade and Joshi (1990). In their case the impeller was located midway in the vessel at C/T = 0.5. In our case the impeller is located closer to the vessel bottom at C/T = 0.3 and the velocity profiles might well be asymmetrical, but no clear literature data was found supporting this suspicion. For the computations with a six-bladed downwards pumping pitched blade turbine (PBT) the velocity and turbulence profiles were prescribed at the bottom surface of the impeller (fig. 1) according to own experimental LDV data.

Further, since the calculated flow patterns are used for calculating the gas transport through the vessel it is necessary to correct the prescribed liquid velocities for the decrease in the dimensionless pumping number N_{qp} of the impeller when the impeller is gassed. This is done assuming that the decrease in pumping capacity of the impeller is proportional to the decrease in power number (Joshi et al, 1982, Trägårdh, 1988):

$$N_{qp,g} = N_{qp,u} \left(\frac{Po_g}{Po_u} \right) \qquad (1)$$

All further information on the geometries investigated, together with the values for the impeller pumping numbers are listed in Table 1.

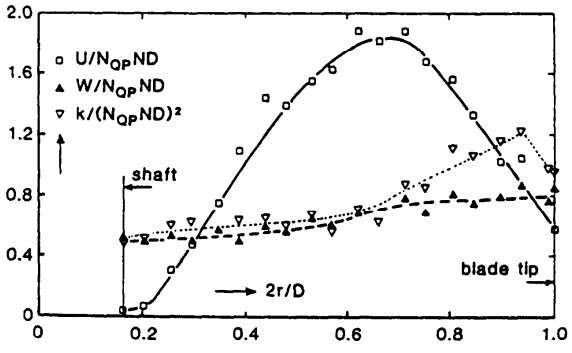

FIGURE 1 Experimental liquid velocities and turbulent kinetic energy in the outflow of a pitched blade turbine.

Table 1, Geometrical information.

	DT	PBT	General
Po_u	5.00	1.55	P/V = 1520W/m^3
Po_g	3.63	1.21	v_{sg} = .0036m/s
$N_{qp,u}$	0.75	0.80	C/T = 0.30
$N_{qp,g}$	0.55	0.63	D/T = 0.40
n	5.55	8.00	D_s/D = 0.75
Fl	.019	.013	S/D = 0.60
			T = 0.444 m

THE GAS-LIQUID MODEL

The flow pattern calculated following the procedure described in the preceding section is used for calculating the transport of the gas through the vessel using the model equations given below.

The continuity equation for the gas-phase reads:

$$\frac{\partial \alpha}{\partial t} + \vec{\nabla}.(\alpha \vec{u}_g) = S_g \qquad (2)$$

S_g denotes the gas source. On performing the Reynolds decomposition and averaging the equation we get for a quasi-steady-state situation:

$$\vec{\nabla}.(\bar{\alpha} \bar{\vec{u}}_g) + \vec{\nabla}.\overline{(\alpha' \vec{u}_g')} = \bar{S}_g \qquad (3)$$

The second term on the left-hand side describes the transport of gas due to turbulent motion of the gas-phase and is not known in general. This leads to a so-called closure problem. This turbulent transport could be modeled by an analogy with the kinetic gas theory. According to this theory the number of collisions per unit time and per unit area between molecules exhibiting random motion and the boundary of a volume element is (1/4) $n \bar{c}$, where $\bar{c}$ is the average velocity of the molecules and n their number density. Since the bubbles in a turbulent gas-liquid dispersion also exhibit random motion we can calculate the turbulent gas flux from one cell into an other by (see also figure 2:

$$\phi_{g,turb} = \frac{1}{4} \bar{\alpha} \overline{|\vec{u}_g'|} \qquad (4)$$

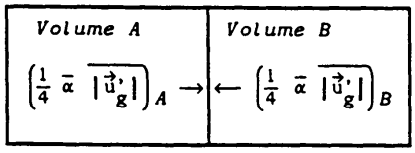

FIGURE 2 Illustration of the turbulent exchange between cells A and B.

Further we assume that the average random fluctuating velocity of the gas phase is proportional to that in the liquid phase:

$$\overline{|\vec{u}_g'|} \sim \overline{|\vec{u}_l'|} = \sqrt{2k} \qquad (5)$$

The linear gas velocity is calculated as the sum of the linear liquid velocity in a single-phase system as calculated with FLUENT and the slip velocity between the two phases:

$$\vec{u}_g = \vec{u}_l + \vec{u}_s \qquad (6)$$

The slip velocity $\vec{u}_s$, in (r, ϕ, z) coordinates can be calculated by a force balance on the bubbles:

$$\vec{F}_s = \left(\rho_l v_b \frac{w^2}{r}, 0, \rho_l g v_b \right) \qquad (7)$$

$$\vec{F}_s = C_D \frac{1}{2} \rho_l |\vec{u}_s| \vec{u}_s \frac{\pi}{4} d_b^2 \qquad (8)$$

The force in the radial direction equals the centripetal force on the bubbles, the force in the vertical direction is of course the buoyancy. The bubbles are assumed to follow the main liquid flow in the circumferential direction, and thus there is no net tangential force on the bubbles.

The constant C_D is a function of bubble Reynolds number and can be calculated from the correlations given by Morsi and Alexander (1972). The bubble Reynolds number is calculated from:

$$Re_b = \frac{\rho_l |\vec{u}_s| d_b}{\eta_e} \qquad (9)$$

Here η_e is the sum of the liquid viscosity and a term proportional to the turbulent viscosity:

$$\eta_e = \eta_l + C_e \rho_l \frac{k^2}{\varepsilon} \qquad (10)$$

This extra term is introduced to account for the decrease in slip velocity when a bubble is moving in a turbulent flow field instead of in a stagnant liquid. A similar approach has already been followed by Barnea and Mizrahi (1975) for the flow in bubble swarms, but in contrast to their work our correction reflects the influence of turbulence in the liquid phase.

A first-order model is used to describe the process of bubble formation in the bulk:

$$\frac{\partial n_b}{\partial t} + \vec{\nabla}.(n_b \vec{u}_g) = \omega(n_{b\infty} - n_b) + S_g / v_{b,in} \qquad (11)$$

The number of bubbles per dispersion volume n_b is related to the gas-holdup and the average bubble volume in the volume element investigated:

$$n_b = \alpha / \langle v_b \rangle \qquad (12)$$

Further $n_{b\infty}$ is the number density of bubbles in which the process of bubble break-up and coalescence would result in case no new bubbles would be added, in other words when the source and convection terms in eq. (12) would be zero. Such a process would result in an average bubble size equal to the maximum stable bubble size according to Hinze (1955):

$$d_{b\infty} = C_{b\infty} \left(12 \frac{\sigma}{\rho}\right)^{3/5} \varepsilon^{-2/5} \qquad (13)$$

The effective coalescence/breakup frequency ω may be proportional to the number of collisions between the bubbles. Another analogy with kinetic gas theory may result in:

$$\omega = C_\omega \frac{3}{2} \sqrt{2} \frac{\alpha}{d_b} \overline{|\vec{u}_g'|} \qquad (14)$$

Equations (11) to (14) are used for calculating the local bubble size in the bulk of the dispersion volume only. For the impeller it is assumed that the impeller breaks up the gas bubbles to the maximum stable bubble size as calculated by eq. (13), on basis of the average energy dissipation rate inside the impeller. Therefore $C_{b\infty}$ could be estimated to be 0.75 from bubble size data reported by Greaves and Barigou (1988).

When the local gas holdup and bubble size are known, the mass transfer coefficient $k_L a_d$ can be calculated by using the equation for k_L given by Kawase and Moo-Young (1990):

$$k_L = 0.301 (\varepsilon \nu)^{1/4} Sc^{-1/2} \qquad (15)$$

The k and ε values as calculated for a single-phase flow by FLUENT (ε_{lp} and k_{lp}) are corrected for the energy input by the gas-phase. The energy input per second for a single bubble is given by:

$$P_b = |\vec{F}_s| . |\vec{u}_s| \qquad (16)$$

Therefore the total energy dissipation rate will be:

$$\varepsilon = \varepsilon_{lp} + \frac{n_b P_b}{\rho_l (1-\alpha)} \qquad (17)$$

Provided that the turbulence as generated by the bubbles has a length scale of the order of the bubble size, and when the turbulent length scale is calculated by:

$$L_t = \frac{k^{3/2}}{\varepsilon} \qquad (18)$$

the total kinetic energy is given by:

$$k = k_{lp} + \left[d_b \frac{n_b P_b}{\rho_l (1-\alpha)} \right]^{2/3} \qquad (19)$$

All the equations above are incorporated in *GHOST!* (Gas Holdup Simulation Tool!). *GHOST!* is capable of calculating local values of void fraction, bubble size, interfacial area and mass transfer. It should be stressed that the computational algorithms are set up in a very flexible way and are not limited to any particular geometry, which means that a quick assessment of the influence of geometrical changes with respect to e.g. sparger position and impeller placement on gas holdup and mass transfer can be made. Further the code allows for prescribing the shape of the gas-holdup profile in the outflow of the impeller. The calculations can be performed on any type of 2D or 3D, uniform or non-uniform, cylindrical finite-difference grid.

EXPERIMENTAL

To verify the calculated single-phase flow patterns several velocity measurements were performed using a TSI Laser Doppler velocimeter, incorporating a 4W Spectra-Physics Argon laser, a fiber optics measurement probe, and a colorburst frequency shifter.

For verification of the calculated gas-holdup profiles, local gas-holdup measurements were performed using a single point optical fiber probe. This measurement method was described by Frijlink (1987).

SINGLE PHASE RESULTS

Figure 3 shows the calculated vector components in the plane midway between two baffles (ϕ = 45°) for a disc-turbine. The computations were done on a 3D grid with 50x25x20 nodes. Due to the radial pumping direction of this impeller the flow is characterized by two main circulation loops, one on each side of the impeller. Such a flow pattern has already been described by numerous authors. This gives confidence in the results.

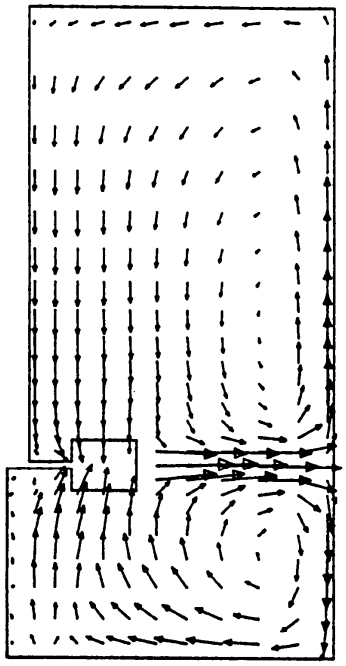

Figure 3 Calculated velocity vectors for a Disc Turbine, midway between the baffles (ϕ = 45°).

Figures 4a,b,c show the flow pattern for a pitched blade turbine as calculated on a 3D grid with 52x27x17 nodes. Figure 4a shows the flow pattern in the plane midway between to baffles (ϕ = 45°). In this plane the flow pattern consists of one large circulation loop, and a small recirculation loop below the impeller. Just in front of the baffle (ϕ = -4°) the flow pattern is approximately the same, although it can be seen that there are differences to be found in the upper half of the vessel. The flow a small distance behind the baffles (ϕ = 15°) is very different from the flow pattern in front of the baffle. It can be seen that a second recirculation loop has formed in the upper half of the vessel, and that the flow along the wall in the upper part of the vessel is directed downwards instead of upwards. The existence of this second recirculation loop has not been reported before in the literature. The fact that such a secondary recirculation loops really exists is shown in figure 5. This figure shows experimental axial liquid velocities as measured in the plane midway between two baffles, near the vessel wall. It can be seen that the axial velocities change sign at a distance of approximately Z/H = 1/3 from the liquid surface, thus proving the existence of this second recirculation loop. The experimental data show that this loop extends at least 45° away from the baffle, whereas the simulations say that the loop extends only approximately 33° from the baffle.

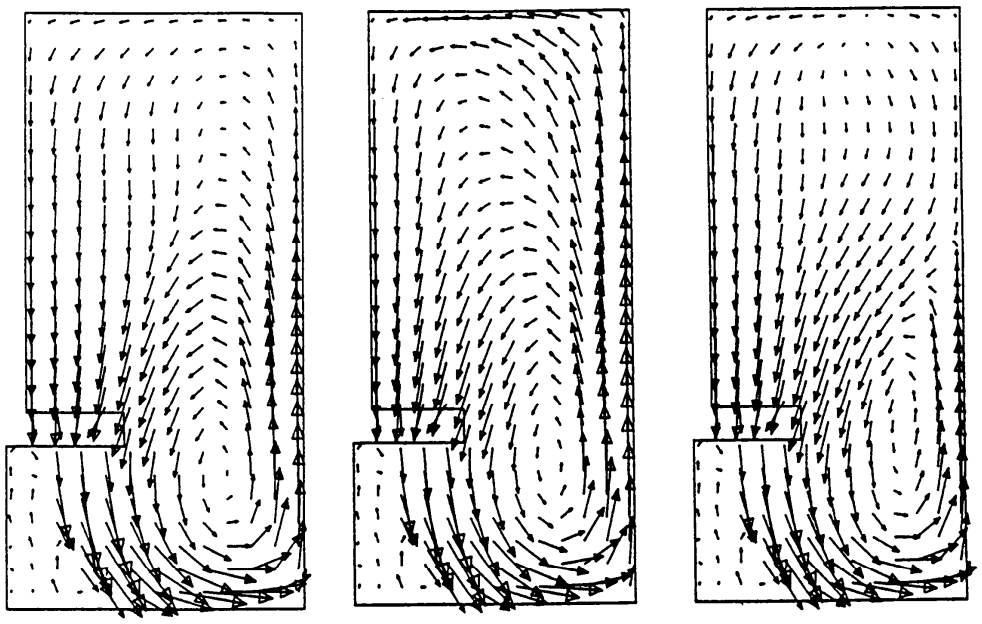

Figure 4a,b,c. Calculated velocity vectors for the PBT, at ϕ = 45°, ϕ = -4° and ϕ = 15°.

This means that the simulated flow patterns are qualitatively correct, showing details not reported before in the literature, but that the quantitative accuracy should be improved even further. It should be mentioned that the recirculation loop was neither found when doing 2D, axisymmetric simulations nor when doing full 3-dimensional simulations with 11 grid nodes in the tangential direction. This might mean that for a correct quantitative prediction of the flow pattern the number of grid nodes in the tangential direction should even be larger than the 17 nodes used in this calculations but due to computational restrictions this could not yet be tested. There may be two reasons for the fact that the existence of such a recirculation loop has not been reported before in the literature. The first reason is that such a loop may not be formed when the impeller is mounted at a larger impeller to bottom clearance. The second reason might be that until now no 3D computations with such a large number of grid nodes were performed.

In general the predicted overall energy dissipation rates compare very well with the total energy input delivered by the impeller, provided that the ASM turbulence model is used. For example with the disc-turbine the calculated total energy dissipation rate in the bulk

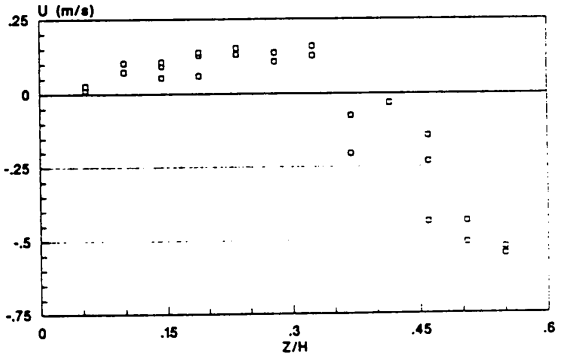

Figure 5 Experimental axial liquid velocities near the wall at ϕ = 45°, for the PBT (n=6Hz).

accounts for 53% of the power input by the impeller. This is quite good, especially since experimental studies report values ranging from 40% to 60% for the hydraulic efficiency (Ranade et. al, 1990). When the k-ε turbulence model is used the predicted energy dissipation rates are about 15% lower than when the ASM model is used.

RESULTS TWO-PHASE SIMULATIONS

Overall results

The set of model parameters with which the two-phase simulations were done are listed in Table 2.

Table 2, Model constants

$C_\bullet$	$C_{b\infty}$	C_ω
0.02	0.75	0.2

With these parameters the simulations and the experimental data were found to match quite well (Table 3), although the overall $k_L a_d$ values tend to be underpredicted. The overall gas holdup is predicted quite accurately. Therefore the too low $k_L a_d$ values might arise from an underestimation of the interfacial area. It should be borne in mind that all calculations are done assuming spherical bubbles. Since the bubbles are possibly ellipsoidal, the surface area will be underpredicted. Further, the number of experimental data is limited and it might turn out that when more experimental data are available, especially with respect to bubble size and bubble shape, the model parameters have to be adjusted.

The reason for the higher gas holdup for the DT lies in the smaller bubble size for this impeller. With the DT the bubbles first enter the impeller, which breaks them up, before they are dispersed. With the PBT the bubbles enter the impeller only after recirculation. This difference in dispersing characteristics leads to a larger bubble size for the PBT. Since larger bubbles have a larger rise velocity, these bubbles will escape from the vessel faster and thus the overall gas holdup will be lower.

Table 3, Experimental and simulation results for the overall holdup (α), overall bubble diameter (d_b) and overall $k_L a_d$.

	α(%)	d_b(mm)	$k_L a_d$ (1/s)
PBT exp.	4.0	-	0.0036
PBT sim.	4.1	3.77	0.0025
DT exp.	4.7	-	0.0038
DT sim.	4.6	3.38	0.0029

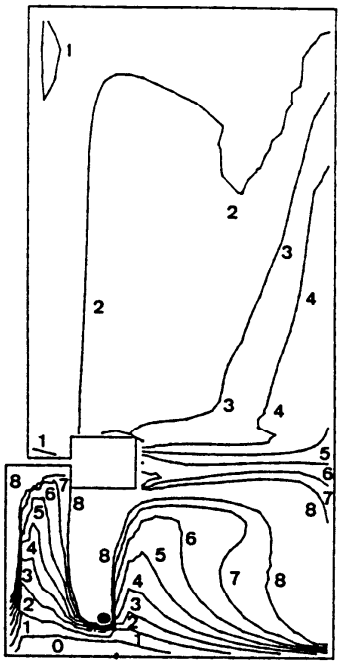

Figure 6. Calculated contours of constant α(%) for the DT at ϕ = 45°

Results Disc Turbine

Figure 6 shows contours of equal gas holdup for the disc-turbine in the plane midway between the baffles. It can be seen that the gas holdup is high near the vessel wall, particularly in the lower part of the recirculation loop where the motion of the rising gas is opposed by the downwards liquid flow. Further the gas holdup shows a peak in the gas flow, issuing from the sparger and rising up into the impeller. For verification of the modeling results several local holdup measurements were performed. Figure 7 shows a comparison between experimental holdup data and simulated holdup data as a function of the radial coordinate 2r/T, at a distance Z/H = 0.92 from the unaerated liquid surface, just above the sparger. It is clear that the rising gas results in a locally high holdup and in a very steep gradient. The holdup rises again near the vessel wall. Figure 8 shows a comparison between experiment and simulation at a constant radius of 2r/T = 0.9, close to the vessel wall. The holdup data have been plotted as a function of the axial coordinate. Both the experimental data and the simulation results show low holdup values near the top surface. The holdup gradually increases with increasing distance to the liquid surface. There is a steep increase in holdup just below the centerplane of the impeller, and a steep decrease again near

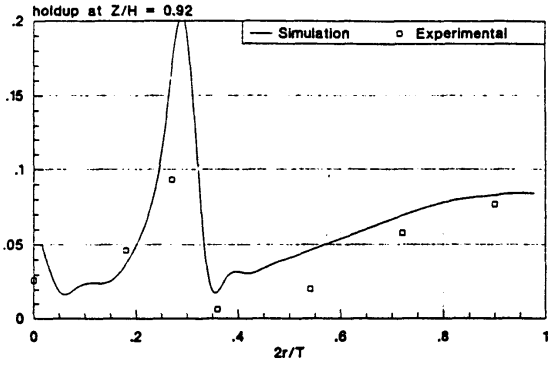

Figure 7 Comparison between experimental holdup data and simulated holdup data (DT).

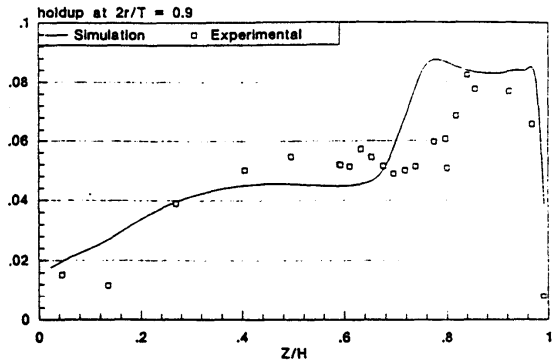

Figure 8 Comparison between experimental holdup data and simulated holdup data (DT).

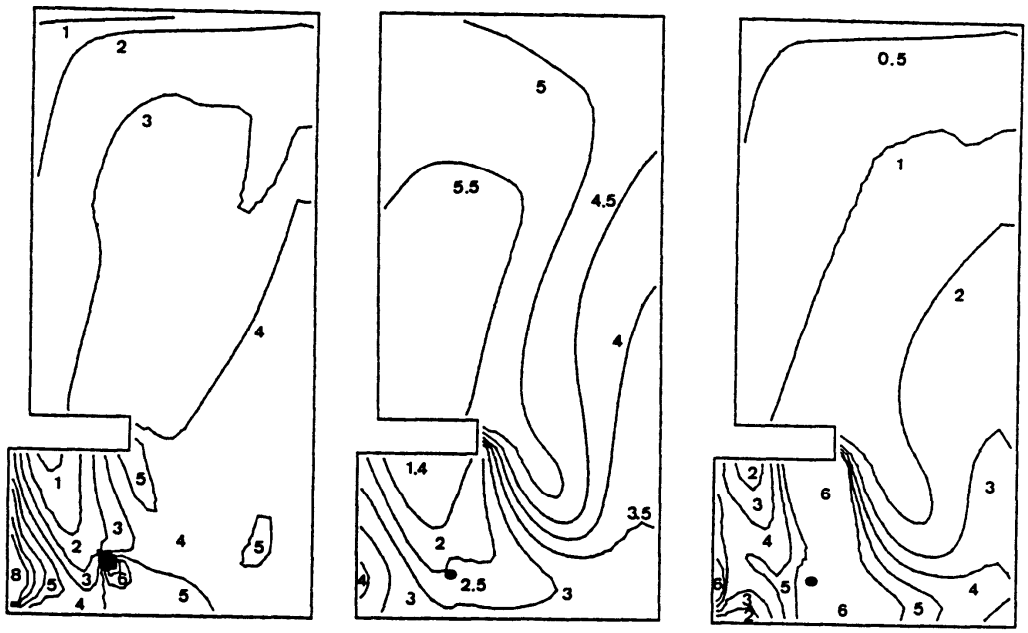

Figure 9a,b,c. Calculated contours of constant α(%), d_b(mm) and $100*k_La_d$ for the PBT at $\phi = 45^o$. The sparger is marked by a black dot. The numbers denote the minimum values in the areas enclosed by the contours.

the vessel bottom. The latter indicates that hardly any gas reaches the bottom. In general the predicted hold-up profiles match the experimental data quite well, thus giving confidence in the modeling method.

GHOST! also predicts the formation of a gas filled vortex in the center of the vessel, below the impeller. In reality such a vortex was not seen. Instead the gas rising from the sparger precesses around the vessel axis with a period of several seconds. Such periodic motions can not be calculated. The fact, however, that it was found that the *GHOST!* solution converged particularly slowly in this region may be an indication of flow instabilities.

Results Pitched Blade Impeller

Figures 9a,b,c show calculated contours of constant holdup, constant bubble size and constant k_La_d respectively, for the PBT. Peaks in the gas holdup are found near the impeller blade tip, near the sparger and, as with the disc turbine, in the center of the vessel, below the impeller. A high .gas holdup is found near

the vessel wall in the lower half of the vessel. Bubble size is small in the outflow of the impeller, and bubble size increases along the circulation loop due to coalescence: the largest bubbles are found above the impeller. The highest $k_L a_d$ values are found in the outflow of the impeller, where the bubbles are small and where k_L is high due to high energy dissipation rates, and near the sparger.

CONCLUSIONS

Three dimensional computations of the single phase flow in a stirred vessel equipped with a PBT, as done with the general purpose code FLUENT, show that a second recirculation loop is formed in the upper part of the vessel, behind the baffles. This has not been reported before in the literature, but is confirmed by own experimental data. When 2D flow calculations are done, or 3D calculations with only a small number of grid nodes in the circumferential direction, this secondary recirculation loop is not found, thus clearly showing the need for 3D simulations.

A model has been presented with which local values of holdup, bubble size and mass transfer can be calculated in a stirred vessel. All the model equations are incorporated in an in-house code named *GHOST!*, that is capable of performing both 2D and 3D computations on any type of cylindrical finite difference grid. The model allows for an assessment of effects on mass transfer, gas holdup and bubble size of impeller type, impeller position, sparger position, aeration rate, etc. Predicted values of local holdup, and overall holdup compare very well with experimental data. Overall mass transfer tends to be underpredicted, but lacking data of local bubble shape make an accurate calculation of the interfacial area difficult. Further research would be useful. Especially more experimental data on local bubble size, local bubble shape, local gas holdup and local mass transfer rate is required, to make an extensive verification of the modeling results possible.

ADDITIONAL NOMENCLATURE

General

- C Distance impeller center to bottom (m)
- C_∞, C_ω, $C_\bullet$ Model constants
- d Diameter (m)
- D_s Sparger diameter (m)
- $\vec{F}_s$ Slip force vector (N)
- k Turbulent kinetic energy ($m^2 s^{-2}$)
- L_t Turbulent length scale (m)
- P Power input (W)
- Po Power number
- r Radial coordinate (m)
- S Distance impeller center to sparger (m)
- S_g Gas source ($m^3 s^{-1}$)
- $\vec{u}_s$ Slip velocity vector
- u Axial velocity (downward positive) (m/s)
- v Radial velocity (m/s)
- w Tangential velocity (m/s)
- v_{sg} Superficial gas velocity (m/s)
- $\langle v \rangle$ Average volume (m^3)
- w Tangential velocity (m/s)
- Z Axial coordinate (0 at surface) (m)
- α Gas holdup
- ϕ Tangential coordinate (0° at baffle)
- ω Effective coalescence/breakup frequency (s^{-1})
- $\eta_\bullet$ Effective viscosity defined by eq. 10

Subscripts

- b Referring to bubble
- g Gas or gassed
- u Ungassed
- lp Referring to single phase
- in At gas input
- ∞ Referring to maximum stable bubble size

REFERENCES

Barnea E., Mizrahi J., Can.J.Chem.Eng. 1975(53)461-469

Boysan F., Selected Topics in Two-Phase Flow, Lecture Series no. 9, Trondheim, may 25-25, 1984

Frijlink J.J., 1987, PhD Thesis, Delft University of Technology, Netherlands

Greaves M., Barigou M., 1988, Proc. 6th Eur. Conf. Mixing, pp 313-320, BHRA, Pavia

Harvey P.S., 1980, PhD Thesis, University of Bath, United Kingdom

Harvey P.S., Greaves M., Trans.I.Chem.E. 1982(60)195-210

Hinze J.O., AIChEJ 1955(1)289-295

Issa R.I., Gosman A.D., Proc. 2nd Int.Conf. Num.Meth.Lam.Turb.Flows, Venice, 1981

Joshi J.B., Pandit A.B., Sharma M.M., Chem.Eng.Sci. 1982(37)813-844

Looney M.K., Issa R.I., Gosman A.D. Politis S. Fifth Int.Conf. on Mathematical Modelling, Berkeley, July 29-31st, 1985

Kawase Y., Moo-Young M., Chem.Eng.J. 1990(43)B19-B41

Mann R., Hackett L.A., 1988, Proc. 6th Eur.Conf. Mixing, pp 321-328, BHRA, Pavia, Italy

Morsi S.A., Alexander A.J., J. Fluid Mechanics 1972(2)193-208

Pericleous K.A., Patel M.K., Physico Chemico Hydrodynamics 1987(8)105-123

Ranade V.V., Joshi J.B., Marathe A.G., Chem.Eng.Comm, 1989(81)225-248

Ranade V.V., Joshi J.B., Trans.I.Chem.E. 1990(68)34-50

Trägårdh Ch., Proc. 2nd Int.Conf.Bioreactor Fluid Dynamics, pp 117-134, BHRA, Cambridge U.K., 1988

REFEREE'S QUESTIONS

1) For your table 1, please give the rotational speed and peripheral speed of the impellers.

	DT	PBT
Rotational speed $n(s^{-1})$	5.55	8.00
Tip velocity (m/s)	3.07	4.42

2) Is the arrow length in figs. 3 & 4 proportional to the local (average) velocity?

The arrow length is indeed proportional to the local average liquid velocity.

3) In fig. 6, is the black dot the gas sparger?

Both in figs. 6 and 9, the gas sparger is marked by a black dot.

4) What is the fluid-dynamic regime for the cases examined in figs. 6 & 9? (At least loading in the former case, probably indirect loading for the latter).

The disc turbine is operated in the loading regime, with vortex/clinging cavities.

The pitched blade turbine is operated in the indirect loading regime and, as far as it could be seen, with clinging/growing cavities.

5) In your opinion, would it be interesting to use a sparger diameter larger than the impeller diameter?

Bakker and Van den Akker (1990) reported for an A315 impeller that the use of a large sparger lead to a decrease in gas-holdup below the impeller and consequently to a more stable gas-handling, but also to a decrease in mass transfer.

Nienow et al. (1988) reported for Rushton turbines with a diameter of D/T = 1/3, that the use of ringspargers with a diameter larger than the impeller lead to an improvement in the performance. Recently, in Delft, we started a case study, in collaboration with prof. A. Lübbert of the University of Hannover, to the gas dispersion performance of a D/T = 1/3 Rushton turbine in combination with a ringsparger with a diameter of 1.9 times the impeller diameter. Preliminary calculations with *GHOST!* showed that this leads to a decrease in the gas loading of the impeller at a slightly larger gas holdup, as compared to a 0.5 D ringsparger mounted close to the impeller. This confirms the results of Nienow et al. However, this work is not finished yet and will be reported later.

REFERENCES

Bakker A., Van den Akker H.E.A., "Gas-liquid contacting with the Lightnin A315 impeller, Effects of flow-pattern", AIChE Annual Meeting, Session on Scale-Up and Industrial Mixing II, November 11 to 16, 1990, Chicago, U.S.A., Unpublished.

Nienow A.W., Allsford K.V., Cronin D., Liu Huoxing, Wang Haozhung, Hudcova V., "The use of large ringspargers to improve the performance of fermenters agitated by single and multiple standard Rushton turbines", 2nd Int.Conf. on Bioreactor Fluid Dynamics, September 21-23, 1988, Cambridge, U.K.